G. M. L. L. da Silva
gisellemlls@terra.com.br
Universidade Federal de Pernambuco
Departamento de Energia Nuclear
50740-540 Recife, PE, Brazil

R. de C. F. de Lima
ritalima@ufpe.br

P. R. M. Lyra
prmlyra@ufpe.br

D. K. E. de Carvalho
dkarlo@uol.com.br
Universidade Federal de Pernambuco
Departamento de Engenharia Mecânica
50740-530 Recife, PE, Brazil

A. Fernandes
afilho@emory.edu
Emory Eye Center
30322 Atlanta, GA, EUA

The Use of an Axisymmetric Formulation of the Finite Volume Method for the Thermal Analysis of the Retina and Ocular Tissues Following Implantation of Retinal Prosthesis

This study analyzes the heat transfer in human eyes following implantation of retinal prostheses using an axisymmetric formulation of the Finite Volume Method. The model used consisted of a vertex centered unstructured grid finite volume method in an edge-based data structure and an explicit time integration. The results of the finite volume thermal analysis in ocular tissues were determined in the presence of two types of retinal implants: subretinal and epiretinal. For the subretinal device, the maximum temperature reached in the retina was 36.78°C (309.78 K) and the irreversible thermal damage occurred at 200 days. In the case of the epiretinal implant, the maximum temperature reached at the retinal/chip interface was 36.92°C (309.92 K) and the irreversible thermal damage occurred at 180 days. Our results indicate that tin spite of its higher dissipation power, the epiretinal implant produces thermal damages similar to that caused by the subretinal implant. The computational tool which was developed was able to effectively calculate temperature profiles and thermal damage values to retinal implants and is also capable to calculate temperature profile in any other geometry of interest, for example with other types s of external thermal source like laser beans.
Keywords: *finite volume method, axisymmetric models, hyperthermia, retina*

Introduction

Some of the leading causes of blindness in the world include conditions such as retinitis pigmentosa (RP) and age-related macular degeneration (AMD). Both involve degeneration of the photoreceptor cells, rendering the visual system to become insensitive to light (Peachey and Chow, 1999). The development of retinal prosthesis is based on the premise that an application of external electrical stimulus can be an alternative approach to potentially restore the function of the visual system (Chow and Chow, 1997; Margalit et al., 2002).

The retinal prosthesis or implant consists in a small chip composed by electrodes that create an electrical current which stimulates adjacent areas in order to activate the visual system. The electrical stimulation of the retina through injection of currents dissipates power and heat. Under normal conditions, the choriocapillaris promotes heat dissipation. In patients with degenerative retinal disorders, the choriocapillaris is damaged. The heat generated by the electronic sensors can damage the adjacent neuronal tissue to the implant sites and also the implant. Furthermore, the increase in temperatures may foster an environment suitable to bacteria proliferation that could potentiate infections (Schwiebert et al., 2002). Energy dissipation and temperatures must be carefully controlled in order to avoid damage to the retina and adjacent tissues which in turn could disturb retinal capillary blood flow. Blood flow disturbance in the retina is a feature of many ocular diseases, including diabetic retinopathy, age related maculapathy and glaucoma (Guan et al., 2003).

Currently, two types s of implants have been developed in the United States, Germany and Japan: an epiretinal and a subretinal. These implants were designed to substitute different physiological functions. The subretinal substitutes the degenerated photoreceptors' cells while the epiretinal stimulates directly the ganglion cells (Margalit et al., 2002). Consequently, the two types of chips are implanted in different places. The subretinal is implanted under the retina's surface, between the pigment epithelium and the photoreceptors cells, while the epiretinal one is placed in contact with the inner surface of the retina (Margalit et al., 2002; Schwiebert et al., 2002; Zrenner, 2002).

In the present work due to the geometrical and physical features of the problem, we have developed and used an unstructured axisymmetric edge-based Finite Volume Method (FVM) to analyze the heat transfer in human eyes in the presence of a retinal implant.

Following this introduction, in the "Physical-Mathematical Model" section, we present the governing equations of the bioheat transfer problem and the expression used to evaluate the damage associated to the burning of living tissues. In sequence, in the "Numerical Modeling" section, we describe the edge-based finite volume formulation used to numerically discretize the partial differential equations that model the bioheat transfer problem. Following, in the "Physical Problem" section, major hypotheses and strategies adopted during the modeling stage are detailed, including the "Thermal Properties and Eye Dimensions" and a description of "The Heat Generation Due to the Retinal Implants". In the "Results" section, we show a "Numerical analysis of the eye with a subretinal device" with the proper "Discussion" of the obtained results and, finally, we present our "Conclusions".

Nomenclature

A	= *Henriques' constant, 3.1 x 1098 s-1*
c	= *tissue specific heat, J/kg.ºC*
cs	= *blood specific heat, J/kg.ºC*
$C_{IJ_L}^{AX(j)}$	= *axisymmetric weighing coefficient*
$D_{IJ_L}^{AX(j)}$	= *axisymmetric weighing coefficient*
ΔEat	= *activation energy, 6.27 x 105 J/mol*
h	= *heat transfer coefficient, W/m2ºC*

Paper received 27 July 2010. Paper accepted 2 September 2011
Technical Editor: Fernando Rochinha

k = *thermal conductivity, W/m°C*
nj = *outward normal directional cosines*
qj = *heat flux at xj direction*
$\overline{q}_n$ = *prescribed heat flux*
$q_{IJ_L}^{j(\Omega^*)}$ = *flux over the domain associated with edge IJ_L*
$q_{IJ_L}^{j(\Gamma)}$ = *flux over the external boundary associated with edge IJ_L*
$q_{IJ_L}^{j(\Gamma_I^*)}$ = *flux over the interfaces of different materials associated with edge IJ_L*

Q = *heat source term*
Qs = *external thermal source term, W/m3*
Q_m = *heat generation of the metabolic heat, W/m3*
Q_p = *heat generation due to blood perfusion, W/m3*
rc = *centroid radius of the control volume*
R = *Universal Constant of gases, 8.31 J/mol.K*
ti = *initial time*
tf = *final time*
T = *temperature, °C*
$\overline{T}$ = *prescribed temperature*
$\hat{T}$ = *temperature calculated by numerical methods*
$\overline{T}^i$ = *initial temperature*
Ta = *arterial blood temperature, °C*
$T\infty$ = *bulk fluid temperature*
$\mathbf{T}$ = *time interval of integration*
xj = *independent space variable*
z = *axial coordinate*

Greek Symbols

ρ = *specific mass, kg/m3*
ρs = *blood specific mass, kg/m3*
ω = *blood perfusion, s-1*
Ω = *analyzed domain*
Ω_D = *damage function, dimensionless*
Γ_C = *boundary subjected to Cauchy or Robin conditions*
Γ_D = *boundary subjected to Dirichlet conditions*
Γ_N = *boundary subjected to Neumann conditions*

Subscripts

a = *relative to arterial blood*
c = *relative to centroid*
I = *relative to node I*
IJ_L = *relative to nodes I and J_L*

Superscripts

j = *relative to direction j*

Physical-Mathematical Model

The Bioheat Transfer Equation, Eq. (1), governs the physical process analyzed.

$$\rho c \frac{\partial T}{\partial t} = k_t \nabla^2 T + Q_p + Q_m + Q_e \tag{1}$$

where ∇^2 is the laplacian operator which can be written in any coordinate system; ρ is the mass density; c is the specific heat; T is the temperature; k_t is the thermal conductivity; Q_e, Q_p and Q_m represents the source (or sink) terms.

In Eq. (1), the source term Q_e represents the external thermal sources, such as lasers or heat dissipated by electronic devices (e.g. retinal implants). The generation term of the metabolic heat (Q_m) can be ignored because, in general, it is smaller than the external heat sources (Sturesson and Andersson-Engels, 1995). The term Q_p is a specific term for the heat generation due to blood perfusion and represents the convective heat removal from the live tissues by the blood vasculature. The referred term is given by Eq. (2) (Diller, 1982; Charny, 1992),

$$Q_p = \omega \rho_s c_s (T_a - T) \tag{2}$$

where ω is the volumetric rate of blood perfusion [m³ of blood/m³ of tissue s], ρ_s and c_s are, respectively, the mass density and specific heat from the blood, T_a is the arterial blood temperature and T is the tissue temperature.

The eye is an organ with a few blood vasculatures. However, there is a large blood flow in the sclera-choroid-retina complex and the retinal blood flow is mainly distributed within the inner retina (Scott, 1988; Guan et al., 2003). In the present work, only the blood perfusion of the retina was considered. The blood flow in the choroid was considered as a convective heat transfer boundary condition between the retina and the choroid, by the use of an adequate heat transfer coefficient (Scott, 1988; Amara, 1995).

The problem described by Eq. (1) was subjected to initial and boundary conditions. The boundary conditions may have been of three different kinds:

a) Dirichlet boundary condition: prescribed temperature $\overline{T}$ over a part of the boundary ΓD.

$$T = \overline{T}, \qquad \text{in } \Gamma_D \text{ X } \mathbf{T} \tag{3}$$

where $\mathbf{T} = [t^i, t^f]$ represented the time interval of integration.

b) Neumann boundary condition: prescribed normal heat flux $\overline{q}_n$ over Γ_N.

$$-q_j n_j = \overline{q}_n, \qquad \text{in } \Gamma_N \text{ X } \mathbf{T} \tag{4}$$

in which n_j were the outward normal directional cosines.

c) Cauchy or Robin boundary condition: mixed boundary condition, i.e., prescribed flux and convection heat transfer over Γ_C.

$$-q_j n_j = \overline{q}_n + h(T - T_\infty), \quad \text{in } \Gamma_C \text{ X } \mathbf{T} \tag{5}$$

with h representing the film coefficient and T_∞ the bulk fluid temperature.

The initial distribution of temperature $\overline{T}^i$ is known for an initial time t^i, so the initial condition was expressed by

$$T = \overline{T}^i \qquad \text{in } \Omega \text{ and } t = t^i \tag{6}$$

A detailed description of the mathematical model can be found in Lyra et al. (2005).

The exposure to high temperatures resulted in irreversible damage to tissue such as protein denaturation, loss of the biological function of molecules and either their evaporation. Denaturation may be seen as the common development that leads to cell necrosis. According to Henriques and Moritz (in: Diller, 1982), the denaturation process is generally described by a particular case of Arrhenius' Law, which is essential to the denaturation/coagulation phenomenon. The kinetics of the thermal denaturation, whose

parameters are the activation energy and temperature, is represented by an integral damage, ΩD, that measures the produced physical damage. For a given damage, the denaturation is determined only by the temporal changes in tissue temperature (Rol et al., 2000).

Initially, Henriques (in: Diller, 1982) determined the values for the pre-exponential constant and the activation energy for tissue burning at low temperatures. These values have been used by several researchers for the analysis of the process of thermal damage.

According to Diller et al. (1991), the threshold burn injuries occur if $\Omega_D = 0.53$, second-degree burn injuries if $\Omega_D = 1$, and third-degree burn injuries if $\Omega_D = 10\,000$.

The damage caused by burning at a certain point of the tissue is given, empirically (Diller et al., 1991), by:

$$\Omega_D = A\int_0^t \exp\left(-\frac{\Delta E_{at}}{RT}\right)dt \tag{7}$$

where A = 3.1 x 10^{98} s-1 , ΔEat = 6.27 x 10^5 J/mol. The universal constant of gases (R) is known as 8.31 J/mol.K and T is the absolute temperature expressed in Kelvin.

Numerical Modeling

The temperature analysis in human eyes was done using an unstructured Finite Volume Method that was developed for solving two-dimensional model problems (Lyra et al., 2004) and later extended to deal with axisymmetric applications (Lyra et al., 2005). Both formulations used a vertex centered finite volume method implemented using an edge-based data structure.

For the axisymmetric formulation, it was convenient to re-write Eq. (1) using a cylindrical coordinates system, which can be expressed by

$$\rho c\frac{\partial T}{\partial t} = \frac{1}{r}\frac{\partial}{\partial r}\left(k\,r\frac{\partial T}{\partial r}\right) + \frac{\partial}{\partial z}\left(k\frac{\partial T}{\partial z}\right) + Q \tag{8}$$

in which all the heat source terms are represented by Q.

By integrating Eq. (8) over a control volume and applying the Finite Volume Method described in Lyra et al. (2005), the semi-discrete equations obtained can be written as

$$\rho c\frac{d\hat{T}_I}{dt}2\pi r_C A_I = -\left(\sum_L C_{IJ_L}^{AX(j)} q_{IJ_L}^{j(\Omega^*)} + \sum_L D_{IJ_L}^{AX(j)} q_{IJ_L}^{j(\Gamma)} + \sum_{k=1}^{2}\sum_L C_{IJ_L}^{AX(j)(R_k)} q_{IJ_L}^{j(\Gamma_I^*)}\right) + Q\,2\pi r_C A_I \tag{9}$$

where the terms $C_{IJ_L}^{AX(j)}$ and $D_{IJ_L}^{AX(j)}$ are the axisymmetric weighing coefficients, A_I is the cross-sectional area of the control volume associated to node I, and r_c is the centroid radius of the control volume.

The first term of the right hand side of Eq. (8) and Eq. (9) quantifies the flux over the interfaces of the control volume associated to node I. The second term quantifies the flux over the boundary faces, and the third one the flux over the interfaces of different materials. The terms $q_{IJ_L}^{j(\Omega^*)}$, $q_{IJ_L}^{j(\Gamma)}$ and $q_{IJ_L}^{j(\Gamma_I^*)}$ represent, respectively, the fluxes over: the domain, the external boundary and over the interfaces of different materials, associated to edge IJ_L.

In order to compute the edges fluxes, it is required to know the nodal fluxes values and, consequently, the values of the nodal gradient of the temperature. The nodal approximation of the gradient is given by

$$\frac{\partial T_I}{\partial x_j}2\pi r_C A_I \cong \sum_L C_{IJ_L}^{AX(j)} T_{IJ_L}^{(\Omega)} + \sum_L D_{IJ_L}^{AX(j)} T_{IJ_L}^{(\Gamma)} - 2\pi b T_I A_I \tag{10}$$

in which b = 1, for radial direction ($x_j = r$) and b = 0 for the axial one ($x_j = z$), and $T_{IJ_L}^{(\Omega)}$ and $T_{IJ_L}^{(\Gamma)}$ are, respectively, the temperature over the domain and over the external boundary associated to edge IJ_L.

The time discretization was done by a simple explicit formulation (Euler forward), where the nodes temperatures were calculated in terms of the adjacent nodal temperatures evaluated at the preview time level.

The time and domain discretization, using triangular meshes, were described in details by Lyra et al. (2005). The discretization included also the adopted approximation for the boundary conditions and the source terms, considering domains with multiple materials.

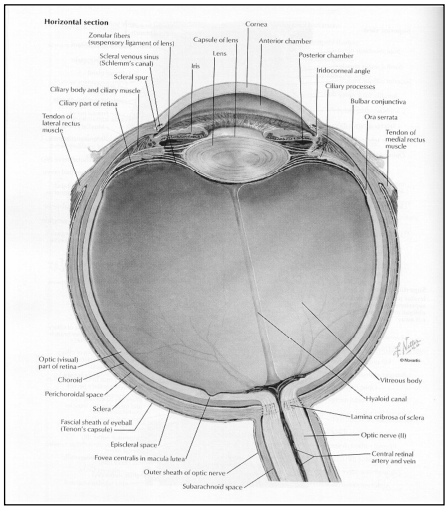

Figure 1. Cross section of the human eye (Netter & Dalley, 1997).

Physical Problem

Considering the cross section of the eye shown in Fig. 1, the following hypotheses have been adopted to simplify the model.

- The use of an axisymmetric model;
- The thermal properties of iris and ciliary body assumed to be equal to those of the aqueous humor (Amara, 1995), so they were considered as a single region;
- Despite the foveae be anatomically different from the retina, it will be considered as a constituent part of the retina;
- Some structures, like nerves, blood vessels, etc., were neglected (Amara, 1995).
- The heat transfer between the external ocular surface and the environment at 293 K occurred by convection;
- The heat transfer in the eye occurred by conduction;
- The heat transfer between retina and choroid occurred by convection;
- The blood temperature was considered equal to 310 K;
- Most of the eye blood perfusion is concentrated at the retina/choroid/sclera complex. So, only the blood perfusion at the retina was considered.

Five regions of different thermal-physical properties were considered (see Fig. 2): the cornea, the aqueous humor, the crystalline lens, the vitreous humor, and the retina.

- The boundary conditions and initial condition were:
- Heat transfer by convection between the ocular external surface and the environment;
- Heat transfer by convection between the retina and the body;

The initial condition considered was the initial temperature distribution inside the eye, without heat sources.

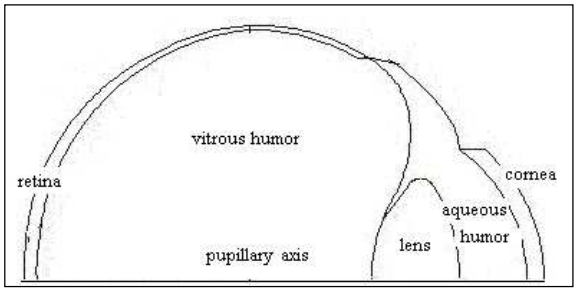

Figure 2. Domain extracted from Fig. 1 using a CAD program.

Before starting the thermal analysis and because of the presence of an external thermal source, it was necessary to calculate the initial condition of the problem. This condition was found by solving Eq. (1) in the steady state case, neglecting the heat source term. It was done by Lima et al. (2005) for an axisymmetric case. Figure 3 shows this temperature profiles along the pupillary axis.

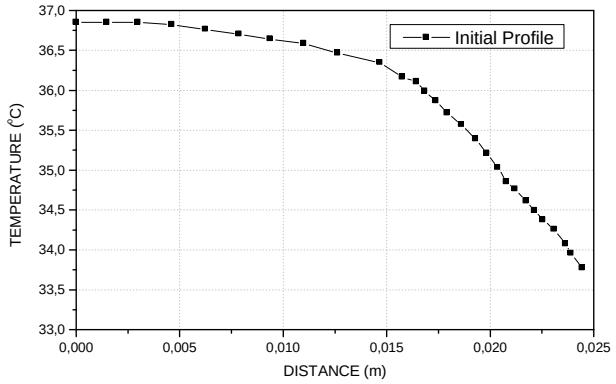

Figure 3. Initial temperature profiles along the pupillary axis.

Thermal Properties and Eye Dimensions

The human eye's dimensions were taken from Amara (1995) and Duane (1987). The pupillary axial diameter of a normal eye was 25.4 mm. The cornea thickness varied from 0.4 mm (at the middle) to 0.7 mm (at the boundary) and the horizontal diameter was 11.8 mm. The lens, located between the aqueous and the vitreous humor, was 4 mm thick and 9 mm in diameter. The retina thickness was 0.2 mm t near the equator, 0.1 mm deep at the fovea and its maximum thickness 0.5 mm, near the optic nerve. Its minimum thickness (0.05 mm) was located at the "ora serrata" (vide Fig. 1). The humors are solutante with different NaCl concentrations, and their vertical lengths were 3 mm for anterior chamber depth and 15 mm for the length of the vitreous humor.

The values of thermal conductivity (k), mass density (ρ) and specific heat (c) were assumed constant within each region of the ocular globe. The thermal properties of the analyzed tissues and of the silicon were presented in Table 1.

Lagendijk (in Scott, 1988) estimated the heat transfer coefficient from the cornea to the environment considering the tear film evaporation and also the heat transfer by radiation and convection to the environment. The value obtained was 20 W/m².K. Lagendijk (In: Scott, 1988) also estimated the heat transfer coefficient from the retina to the choroid as 65 W/m².K. This value includes the heat losses due to the blood perfusion in the choroid region.

Table 1. Thermal properties of eye's tissues.

Tissue	*k (W/mK)* [(a)]	*ρ (kg/m³)* [(a)]	*c (J/kgK)* [(a)]	*ω (s⁻¹)* [(b)]
Cornea	0.580	1050	4178	---
Aqueous Humor	0.580	1000	3997	---
Lens	0.400	1050	3000	---
Vitreous Humor	0.603	1000	4178	---
Retina	0.628	1000	4190	0.012

[(a)]Scott, 1988 [(b)] Welch et al., 1980.

The Heat Generation Rate Due to the Retinal Implants

The heat generation rate presented in the problem is caused by the implanted chip at the retina. Both types of retinal implants: the epiretinal and subretinal have their own specific heat generation rate.

The present simulation values used general data available in literature (Hämmerle et al., 2002; Clements et al., 1999).

The implants are based on a silicon chip with a passivation layer, made of silicon oxide, which encapsulates the chip. The chips carry hundreds to thousands of light-sensitive microphotodiodes equipped with microeletrodes of gold or titanium nitride. The devices are implanted near to the macula.

In vivo tests it was used chips in which duration between implantation and explantation ranged up to 18 months, although chips incurred considerable morphological damage when implanted for more than 3 months. After 6 months, the passivation layer becomes very thin due to chemical degradation and after 12 months a considerable damage to the silicon is observed, while the electrodes do not show any detectable sign of morphological damage (Hämmerle et al., 2002).

For the subretinal device, we used the values obtained by Hämmerle et al. (2002). The chip diameter was 3 mm and its thickness was 70 μm. The chips' resistance was 1000 Ω and had a current delivery of 0.05 mA. The power dissipation was equivalent to 2.5×10^{-6} W.

For the epiretinal one, we used the data from Clements et al. (1999). The implant's area was 4.6 x 4.7 mm² and 30 μm. The power dissipation to the retina was 60 mW.

The temperature profiles were analyzed for both cases during a period of time that varied from three to six months. All values were obtained assuming that the implants were fully charged during the period of the analyses.

Results

The computational domain of interest is obtained from Fig. 1 using a CAD program. The geometry simplifications discussed in the previous section were used. Due to the "quasi-axisymmetric" nature of the problem, an axisymmetric model was adopted, so only

a half of a 2-D cross section of the domain needed to be analyzed. Figure 2 shows the referred domain and the regions of interest.

In order to discretize arbitrary two-dimensional domains, we used a computational system developed by Lyra and Carvalho (2000), which can generate triangular, quadrilateral and mixed consistent meshes. In the present work, we used triangular unstructured meshes. The adopted mesh generator, as any conventional unstructured mesh generator, provided the mesh data in an element-based data structure. The implementation of the finite volume solver required a pre-processing stage in order to convert the element-based data structure into an edge-based one. After the pre-processor stage finished, the element-based data structure could be discarded. After this stage, the edge-based data structure and the physical properties were fed to a FVM computational solver. The temperature profile and the damage function historic values were then obtained from the FVM computational tool.

Numerical Analysis of the Eye with a Subretinal Device

The maximum calculated temperature in the retina was 36.78°C (309.78 K). The new steady-state was reached at 70 s and the corresponding damage function value was 4.7 x 10^{-7}. The thermal damage reached the value of 0.53 at 107 days. The thermal damage reached the value of 1 (irreversible damage) at 200 days. Figure 4(a) shows the temperatures contours of the eye with the subretinal device after the new steady-state was reached.

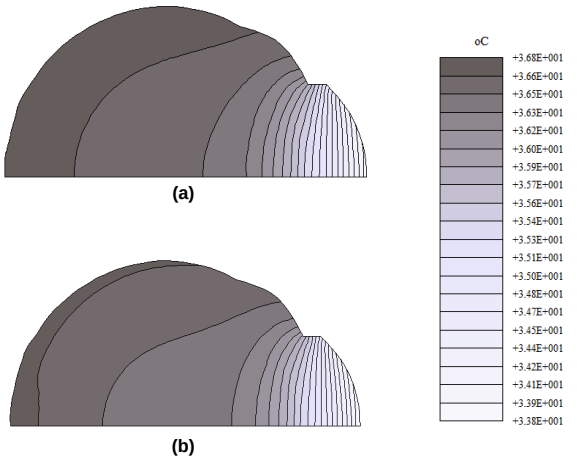

Figure 4. Temperature contours for an eye with: (a) a subretinal device; (b) an epiretinal device.

Numerical Analysis of the Eye with an Epiretinal Device

The maximum temperature at the retinal/chip interface was 36.92°C (309.92 K). The new steady-state was reached after 8.2 s and the corresponding damage function value was 5 x 10^{-7}. The thermal damage reached the value of 0.53 at 94 days. The thermal damage reached the value of 1 (irreversible damage) at 180 days. Figure 4(b) shows the temperature contours of the eye with the epiretinal device after the new steady-state was reached.

Figure 5 shows the behavior of the damage function for both kinds of implants during a period of approximately 3 months after the implantation.

Discussion

In spite of the fact that the electrical power density for the epiretinal implant was approximately 2700 times higher than that of the subretinal, the difference in temperatures at each stationary stage of the process was not different (less than 0.2%). Irreversible thermal damage to cells occurred within a short difference of time between the two implants.

These results were expected due to the relationship of the epiretinal implant with the vitreous humor, which has a greater capacity to dissipate the heat generated by this implant (Margalit et al., 2002).

After the chip implantation, a new steady state was quickly reached in both cases. Then, the increase of the thermal damage was calculated for the new constant temperatures, by the exponential expression shown in Eq. (7).

A brief sensitivity analysis of the damage variation with temperature was performed and is shown in Tables 2 and 3, for the subretinal and the epiretinal implants, respectively.

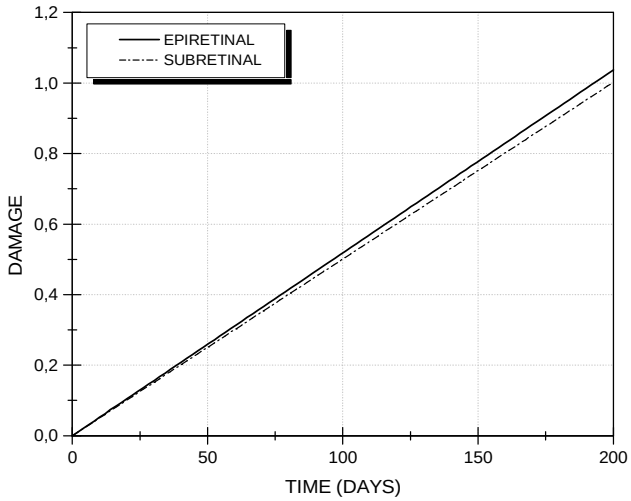

Figure 5. Comparison between damage function values of the two kinds of implants.

Table 2. Sensitivity analysis of the thermal damage with the temperature of the subretinal implant.

Temperature (Kelvin)	Temperature (°C)	Δ (%)	Time for Ω = 0.53	Time for Ω = 1
306.68	33.68	–1	3.8 years	7.2 years
308.23	35.23	–0.5	400 days	760 days
309.78	36.78	-	107 days	200 days
311.33	38.33	+0.5	35 days	67 days
312.88	39.88	+ 1	10 days	20 days
325.27	52.27	+ 5	1.5 days	3 days

Table 3. Sensitivity analysis of the thermal damage with the temperature of the epiretinal implant.

Temperature (Kelvin)	Temperature (°C)	Δ (%)	Time for Ω = 0.53	Time for Ω = 1
306.82	33.82	- 1	3.4 years	6.4 years
308.37	35.37	-0.5	360 days	680 days
309.92	36.92	-	94 days	180 days
311.47	38.47	+0.5	31 days	60 days
313.02	40.02	+ 1	9 days	18 days
325.42	52.42	+ 5	1.4 days	2.6 days

As it is well known, the temperature profiles obtained by any numerical simulation are approximations of real cases. Moreover, the values of the thermo-physical parameters of live tissues are also

not very precise. As it can be seen on Tables 2 and 3, even small variations (approximately 0.5%) of the calculated temperatures can cause a large variation on the time to reach the irreversible damage, as expected. More reliability could be achieved by the numerical simulation if real values for the implants were available.

As soon as more information regarding the electrical power of the implants become available, the developed computational tool can be used to investigate deeply these features.

Conclusions

The new technology of retinal implants has motivated the present study. Although basic investigations in animals are underway presently, the implants are being used simultaneously in blind people and in animals and further investigations of possible long term side effects are paramount.

The results obtained in the present work indicate that the epiretinal device, despite having higher power dissipation, produces thermal damages similar to that caused by the subretinal implant. This fact demonstrates the higher capacity of the epiretinal device in heat dissipation, which may be explained by its relationship to the vitreous humor.

As expected, the computational tool developed was capable to effectively calculate the temperature profiles and thermal damage values in ocular tissues with retinal implants. This tool is also capable to calculate temperature profile in any other geometry of interest and with other kind of external thermal source like laser sources (Lima et al., 2006).

Acknowledgements

The authors would like to acknowledge the Brazilian Research Council (CNPq), the National Petroleum Agency (ANP) and (CAPES) for the financial support provided during the development of this research.

References

Amara, E.H., 1995, "Numerical investigations on thermal effects of laser-ocular media interaction", *Int. J. Heat Mass Transfer*, Vol. 38 (13), pp. 2479-2488.

Charny, C.K., 1992, "Mathematical models of bioheat equation". In: *Advances in Heat Transfer: Bioengineering Heat Transfer*. Edited by CHO, YI, Academic Press, Inc. 1, Vol. 22, pp. 19-155.

Chow, A.Y., Chow, V.Y., 1997, "Subretinal electrical stimulation of the rabbit retina", *Neuroscience Letters*, Vol. 225, pp. 13-16.

Clements, M., Vichienchom, K., Liu, W., McGucken, E., DeMarco, C., Hughes, C., Mueller, J., Humayun, M., De Juan, E., Weiland, J., Greenberg, R., 1999, "An implantable neuro-stimulator device for a retinal prosthesis", *In IEEE International Solid-State Circuits Conference.*

Diller, K.R., 1982, "Modeling of bioheat transfer processes at high and low temperatures", In: *Advances in Heat Transfer: Bioengineering Heat Transfer*. Edited by CHO, YI. Academic Press, Inc., Vol. 22, pp. 157-357.

Diller, K.R., Hayes, L.J., Blake, G.K., 1991, "Analysis of alternate models for simulating thermal burns", *Journal of Burn Care & Rehabilitation*, pp. 177-189.

Duane, T.D., Jaeger, E.A., 1987, *Biomedical foundations of ophthalmology*, Vol. 1, Ed. Harper & Row.

Guan, K., Hudson, C., Flanagan, J.G., 2003, "Variability and repeatability of retinal blood flow measurements using the Canon Laser Blood Flowmeter", *Microvascular Research*, Vol. 65, pp. 145-151.

Hämmerle, H., Kobuch, K., Kohler, K., Nisch, W., Sachs, H., Stelzle, M., 2002, "Biostability of micro-photodiode arrays for subretinal implantation", *Biomaterials*, Vol. 23, pp. 797-804.

Lima, R. de C.F. de, Lyra, P.R.M., Silva, G.M.L.L. da, Carvalho, D.K.E. de, 2004, "Análise térmica dos tecidos oculares dotados de implantes retinianos através da utilização do método dos volumes finitos em malhas não-estruturadas". In Proceedings of CILAMCE 2004 - Iberian Latin American Congress on Computational Methods in Engineering, Recife, published in CD-ROM.

Lima, R. de C.F. de, Lyra, P.R.M., Guimarães, C.S.C., Carvalho, D.K.E. de, Silva, G.M.L.L. da, 2006, "Modelagem computacional da biotransferência de calor no tratamento por hipertermia em tumores de duodeno através do método dos volumes finitos em malhas não estruturadas", *Revista Brasileira de Engenharia Biomédica*, 22(2), pp. 119-129.

Lima, R. de C.F. de, Lyra, P.R.M., Guimarães, C.S.C., Carvalho, D.K.E. de, 2004, "An edge-based unstructured finite volume procedure for the numerical analysis of heat conduction applications", *J. of the Braz. Soc. of Mech. Sci. & Eng.*, Vol. 26(2), pp. 160-169.

Lyra, P.R.M., Carvalho, D.K.E. de, 2000, "A Flexible unstructured mesh generator for transient anisotropic remeshing", In Proceedings of the ECCOMAS 2000 – European Congress on Comp. Meth. in Applied Sciences and Eng., Barcelona, published in CD-ROM.

Lyra, P.R.M., Lima, R. de C.F. de, Guimarães, C.S.C., Carvalho, D.K.E. de, 2004, "An edge-based unstructured finite volume procedure for the numerical analysis of heat conduction applications", *J. of the Braz. Soc. of Mech. Sci. & Eng.*, Vol. 26(2), pp. 160-169.

Lyra, P.R.M., Lima, R. de C.F. de, Carvalho, D.K.E. de, Silva, G.M.L.L. da, 2005, "An axisymmetric finite volume formulation for the solution of heat conduction problems using unstructured meshes", *J. of the Braz. Soc. of Mech. Sci. & Eng.*, Vol. 27(4), pp. 407-414.

Margalit, E., Maia, M., Weiland, J.D., Greenberg, R.J., Fujii, G.Y., Torres, G., Piyathaisere, D.V., O´Hearn, T.M., Liu, W., Lazzi, G., Dagnelie, G., Scribner, D.A., de Juan Jr., E., Humayun, M.S., 2002, "Retinal prosthesis for the blind", *Survey of Ophthalmology*, Vol. 47(4), pp. 335-356.

Netter, F.H., Dalley II, A.F., 1997, *Atlas of Human Anatomy*, 2nd ed., Novartis, USA.

Peachey, N.S., Chow, A.Y., 1999, "Subretinal implantation of semiconductor-based photodiodes: progress and challenges", *Journal of Rehabilitation Research and Development*, Vol. 36(4).

Rol, P., Fankhauser, F., Giger, H., Dürr, U., Kwasniewska, S., 2000, "Transpupillar laser phototherapy for retinal and choroidal tumors: a rational approach", *Graefe's Arch. Clin. Exp. Ophthalmolog.* , Vol. 238, pp. 249-272.

Schwiebert, L., Gupta, S.K.S., Auner, P.S.G., Abrams, G., Lezzi, R., Mcallister, P., 2002, "A biomedical smart sensor for the visually impaired", *IEEE Sensors*, paper No. 62-2.

Scott, J.A., 1988, "A finite element model of heat transport in the human eye", *Phys. Med. Biol.*, Vol. 33 (2), pp. 227-241.

Sturesson, C., Andersson-Engels, S., 1995, "A mathematical model for predicting the temperature distribution in laser-induced hypertermia. Experimental evaluation and applications", *Physics in Medicine and Biology*, Vol. 40(12), pp. 2037-2052.

Welch, A.J., Wissler, E.H., Priebe, L.A., 1980, "Significance of blood flow in calculations of temperature in laser irradiated tissue", *IEEE Transactions of Biomedical Engineering*, BME-27 (3), pp. 164-166.

Zrenner, E., 2002, "Will retinal implants restore vision?", *Science*, Vol. 295, pp. 1022-1025.